ON THE DEGRADATION OF ACOUSTIC ANGLE-OF-ARRIVAL ESTIMATES DUE TO ATMOSPHERIC TURBULENCE

D. Keith Wilson
Acoustics Team, Battlefield Environment Division, U. S. Army Research Laboratory
ATTN: AMSRL-IS-EE, 2800 Powder Mill Road, Adelphi, MD 20783-1197

Abstract

The ability of an acoustic array to accurately track sources is limited primarily by background noise and by atmospheric turbulence. Modeling of the latter effect is the main topic of this paper. The turbulence degrades angle-of-arrival (AOA) estimates by creating uncorrelated phase and amplitude fluctuations at the individual array elements. Theoretically optimal array performance can be determined by calculating Cramer-Rao lower bounds (CRLB 's) on the AOA estimates. CRLB calculations are presented in this paper for several different turbulence models and propagation environments. It is shown that the turbulent degradation becomes quite important in low signal-to-noise scenarios, particularly for propagation distances greater than several hundred meters and acoustic frequencies above 50 Hz. The reduction in array coherence is found to be caused almost exclusively by along-path wind velocity fluctuations generated by near-ground wind-shear instabilities. Large turbulence structures, such as boundary-layer thermals characteristic of a sunny day, may play an indirect role by creating regions of locally high shear near the ground. A theory for propagation through such intermittent turbulence is used to show that accuracy of AOA estimates can fluctuate by several degrees, depending on whether the propagation is through a locally active region of turbulence or not.

1. Introduction

Acoustic sensor arrays have long been used to detect, locate, and identify objects m the ocean. In the atmosphere, however, these roles are more often performed by radar and optical systems than by acoustical ones. The primary reason for this state of affairs is simple: sound waves are minimally attenuated when they propagate through water, but strongly so through air; the situation is essentially reversed for electromagnetic (EM) waves.

Given such a fundamental physical constraint, it may seem surprising that there has been renewed interest and activity during recent years in the development of acoustical systems for atmospheric battlespaces. Systems under development by the U.S. Army that incorporate acoustical arrays include the Brilliant Antitank Munition (BAT), the Remote Sentry, the Wide Area Mine (WAM), and the Intelligent Minefield (IMF). There are several reasons why acoustical systems have overcome their inherent limitations to achieve this new popularity. For one, they are relatively inexpensive and simple to design, a benefit attributable in no small part to modern capabilities in digital signal processing. This makes it feasible to deploy them in large numbers. Acoustical systems also are unaffected by smoke and other obscurants that hamper optical systems. They furthermore do not necessarily require a line-of-sight propagation path, since sound energy often readily penetrates into shadow regions by diffraction and turbulent scattering. Although acoustical systems never will completely supplant the dominant EM technologies, it does appear that they can beneficially supplement existing EM systems, in many cases providing additional, useful information on the battlefield.

One important characteristic of acoustic arrays deployed in the atmosphere is that their performance depends strongly upon atmospheric conditions. Performance is normally enhanced by still, nighttime conditions, and degraded by atmospheric turbulence occurring during windy conditions or on a sunny day. This is because array beamforming relies on good mutual coherence between the signals received by the individual sensors; turbulence causes a loss of such coherence. Effective deployment of acoustic arrays requires understanding and quantification of this turbulent degradation.

This paper describes a theoretical framework for analyzing turbulence effects on acoustic arrays that are used to determine source bearings. Some example calculations of array performance are given for typical atmospheric conditions.

2. General Procedure and Assumptions

As shown in Fig. 1, the analysis of turbulence effects on sensor arrays involves many sub-problems: it requires adequate characterization of atmospheric conditions, a realistic turbulence model, a realistic background noise model, a suitable theory for acoustic propagation through turbulence, and statistical methods from estimation theory. Because of the complex nature of the problem, it is impossible to explore all of the important issues here. I will focus on the turbulence modeling, and simplify many other aspects of the problem,

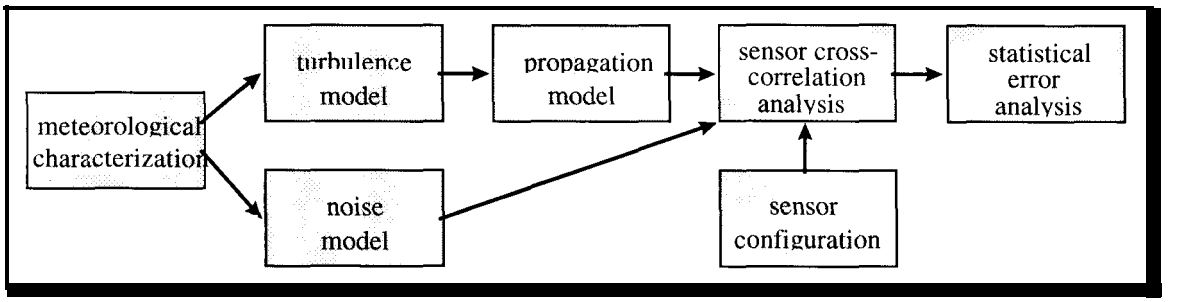

Figure 1: Interrelationships of the many sub-problems involved in *the* analysis of acoustic sensor *array performance in the atmosphere.*

One simplifying assumption I make is that the noise at the individual sensors is uncorrelated and equal in variance. This is probably not a good assumption, in general: the sources of noise that are usually most significant, such as other battlefield participants and wind-induced pressure fluctuations, undoubtedly produce correlated noise. Much remains to be learned regarding the realistic modeling of these noise sources.

I will also assume that the acoustic propagation may be approximated by plane waves. This is quite reasonable if the size of the array is small compared to its distance from the source.

In this paper I make the distinction between *angle-of-bearing* and *angle-of-arrival. Angle-of-bearing (AOB)*, of course, refers to the actual direction of the source. *Angle-of-arrival (A OA)* refers to the orientation of the wavefront normal when the sound reaches the array. For horizontal arrays the two angles are usually nearly the same. The situation is quite different for vertical arrays, however, as shown in Fig. 2. In this case refraction of the sound normally causes the AOA and AOB to be different. For downwind propagation, there are typically multiple ray paths and hence a distribution of AOA's. For upwind propagation, the AOA is normally determined by the location of the "scattering volume," i.e., the region from which the sound energy reaching the source was scattered by turbulence.

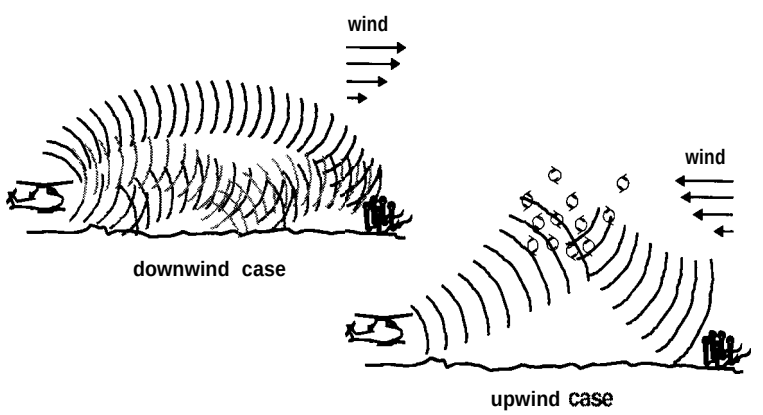

Figure 2. The effect of refraction on the acoustic wavefront angle-of-arrival. In the downwind (or in the temperature inversion) case, multiple arrivals are created. In the upwind (or in the temperature lapse) case, the sound reaching the receiver is normally scattered there by turbulence.

Because of the refraction effects, most of the existing acoustic systems only attempt to determine horizontal source bearings. It is possible that reasonable vertical bearings could be obtained if a refraction model were incorporated into the analysis. In this paper I circumvent the refraction issue by explicitly considering the accuracy of AOA estimates; the reader should keep in mind that if vertical bearings are the concern, the AOA estimate may not be useful without additional information.

3. Sensor Cross Correlation Analysis

It is perhaps easier to discuss the steps shown in Fig. 1 in essentially reverse order. We will start with the sensor cross correlation analysis, and the ensuing statistical analysis of AOA errors. The derivation in this section is similar to one given recently by Song and Ritcey (1996), for the case of ocean acoustic arrays.

The received signal at each sensor has contributions from the source of interest, whose sound arrives at the angle ψ, as well as from all other sources (the "noise"). Hence the total signal $\mathbf{p}(\psi,t)$ consists of additive contributions from the source $\mathbf{s}(\psi,t)$ and the noise $\mathbf{n}(t)$:

$$\mathbf{p}(\psi,t)=\mathbf{s}(\psi,t)+\mathbf{n}(t),$$

where *t is* time, and the holding indicates an N x 1 column vector, N being the number of array elements. Assuming that the source signals have been normalized to unit variance, that the signal and noise are mutually uncorrelated, and that the noise at each of the sensors is equal in variance, we have

$$\mathbf{R}_{pp}(\psi) = (PA^*) = \mathbf{R}_{ss}(\psi)+\sigma_n^2\mathbf{I},$$

where σ_n^2 is the noise variance, and I is the identity matrix. The signal-to-noise ratio is by definition

$$\mathrm{SNR} = -10\log\sigma_n^2.$$

The source signal cross correlation matrix $R_{ss}(\psi)$ is approximately equal to the element-by-element product of an array steering matrix $\mathbf{S}(\psi)$ and a mutual coherence matrix T. The elements of these two matrices are, respectively,

$$S_{mn}(\psi) = \exp\left[-ikd_{mn}\cos(\psi-\alpha_{mn})\right]$$
$$T_{mn}=\Gamma(d_{mn})$$

in which *k is* the acoustic wavenumber, d_{mn} *is* the distance between sensors *m* and *n* and α_{mn} the angle between them (see Fig. 3). The function Γ is called the mutual coherence function (MCF), and will be discussed in the next section.

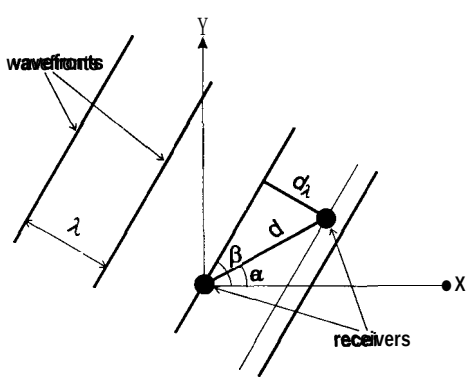

Figure 3. Planar *wavefronts* incident *on* a *pair of receivers. The distance between the sensors is d and the angle is* α.

According to the Cramer-Rao theorem, the mean-square error in an angle of arrival estimate $\hat{\psi}$ is always greater than or equal to the inverse of the Fisher information matrix $\mathbf{J}(\psi)$:

$$\left\langle(\psi-\hat{\psi})^2\right\rangle \geq \mathbf{J}^{-1}(\psi),$$

In our case the Fisher matrix is given by the following matrix product (Song and Ritcey, 1996):

$$\mathbf{J}(\psi) = M\mathrm{tr}\left(\mathbf{R}_{pp}^{-1}\frac{\partial\mathbf{R}_{pp}}{\partial\psi}\mathbf{R}_{pp}^{-1}\frac{\partial\mathbf{R}_{pp}}{\partial\psi}\right),$$

where *M is the* number of statistically independent samples used to estimate the sensor cross correlations (i.e., the number of applications of the beamformer prior to averaging).

The inverse of the Fisher matrix is called the *Cramer-Rao Lower Bound* (CRLB). The CRLB gives the lowest mean-square error that is theoretically obtainable. That is, if we had the best possible algorithm for converting the sensor phase information to AOA estimates, the mean-square error of our estimates would equal the CRLB. Fortunately it appears that practical methods yield performance comparable to the CRLB (Song and Ritcey, 1996). Actually, in the rest of this paper, when I mention the CRLB I will actually mean its square root. This quantity corresponds to the best obtainable root-mean-square error, and is more natural to deal with since its dimensions are linear rather than squared.

4. Propagation Model

The MCF needed for the sensor cross correlation analysis is equal to the coherence between the signals at two receivers. In the case of plane-wave propagation, the MCF is approximately (Rytov *et al.*, 1989)

$$\Gamma(\rho) \cong \exp\left\{-\frac{\pi k^2 X}{2}\left[b(0)-b(\rho)\right]\right\},$$

where X is the propagation distance, ρ is the separation between the receivers, and b(P) is the two-dimensional (2D) correlation function (sometimes called the transverse correlation function). The 2D correlation can be found from the 3D correlation *R* using the equation

$$b(r_2,r_3)=\frac{1}{2\pi}\int_{-\infty}^{\infty} R(r_1,r_2,r_3)\,dr_1,$$

in which r_1 is in the direction of propagation, and r_2 and r_3 *are* the two transverse directions. For isotropic turbulence $\rho^2 = r_2^2 + r_3^2$, and $b(r_2,r_3) = b(p)$. If the turbulence is anisotropic, the MCFgenerally becomes afunctionof r_2 and r_3 instead of just *p*.

In order to better compare the behavior of the MCF corresponding to various turbulence models, it is worthwhile to define a *two-dimensional structure function (TSF)* $d(\rho)$ such that

$$d(p) = 2\left[b(0)-b(\rho)\right].$$

The TSF is the 2D counterpart of the usual 3D structure function. A quantity that is also closely related to the 2D correlation and useful when comparing turbulence models is the *integral length scale,* $\mathcal{L}$:

$$\mathcal{L}=\frac{1}{\sigma^2}\int_0^{\infty} R(r)\,dr=\frac{\pi}{\sigma^2}b(0)\cdot$$

If the source of the coherence loss is fluctuations in the sound speed, then the MCF should be computed using the 2D correlation function for the index of refraction N, where

$$N \approx -2c'/c_0 \approx -T'/T_0,$$

T being the temperature, (Primes indicate fluctuations, and the subscript "O" indicates the mean value.) For acoustic propagation in the atmosphere, however, it is most frequently the situation that the coherence loss is caused by fluctuations in the along-path wind speed υ_1. In this case the correlation function of

$$u_1 = -2\upsilon_1/c_0$$

is to be used (Ostashev, 1994). The situation for wind speed fluctuations is further complicated by the fact that correlation functions for an isotropic, homogeneous, solenoidal vector field are not interchangeable with those for a scalar field. For example, the functional form of b(p) for the scalar Gaussian model differs from the vector Gaussian model. These issues are beyond the scope of this paper, however; the reader is referred to Batchelor (1953) and Wilson (1996) for details.

5. Turbulence Models

The turbulence model plays a critical role in determining the MCF. A fully 3D turbulence model is required for the computation. Unfortunately, most existing correlation and spectral equations for atmospheric turbulence are ID in nature, since they are based on measurements made from stationary towers.[1] As a result we are forced to consider highly idealized turbulence models that, although they may lack realism, are at least 3D.

The simplest model is the isotropic *Gaussian* model. It is quite easy to handle analytically, and is not completely unreasonable for the large, energetic eddies in the turbulence, called the *energy subrange. The* disadvantage of the Gaussian model is that it does not realistically describe the turbulent *inertial subrange (the* eddies participating in the cascade of energy from large to very small scales). This is a serious problem with regard to array performance evaluation, since the inertial scales are usually comparable to the spacing between the microphones.

A much better model than the Gaussian is the *von Kármán*. Like the Gaussian model, the von Kármán model is reasonable for the energy subrange. The main benefit of the von Kármán model is that it also works very well in the inertial subrange. Although it is more analytically difficult to handle the Gaussian model, closed-form results can still be obtained using the von Kármán model.

Like the von Kármán model, the *Kolmogorov* model is valid in the inertial subrange. It has the additional advantage of simplicity, The disadvantage is that it is based on scaling laws that are *only* valid in the inertial subrange, being inapplicable to the energy subrange. We will see that the energy subrange structure of atmospheric turbulence does affect acoustic arrays in significant ways.

The final model we will consider is the Wilson and Thomson (1993), anisotropic, Gaussian model. Due to its Gaussian nature the Wilson and Thomson model is poor for the inertial subrange. However, it attempts to capture realistic anisotropic features characteristic of atmospheric turbulence. It is interesting to compare the Wilson and Thomson model to the isotropic Gaussian model, in order to learn about the significance of the anisotropy.

Basic equations for the different models are listed in Fig. 4. The Gaussian, von Kármán, and Kolmogorov models are plotted for comparison in Fig. 5.

6. Example Calculations

All of the example calculations we will consider are for five element uniform-line arrays. The wavefront incidence is assumed to be broadside ($\beta = \alpha$ in Fig. 3).[2] Furthermore, in the CRLB calculations there are assumed to be M=5 independent samples.

Figure 6 shows the compares the CRLB from the scalar Gaussian and von Kármán models, as a function of the spacing between the array elements and the total index-of-refraction variance. The SNR in both cases was 20 dB, and the integral length scale was chosen such that $\mathcal{L}=5\lambda$, where λ is the acoustic wavelength. The length of the propagation path was 50 $\mathcal{L}$.

One can conclude from the Fig. 6 that, at least for this propagation distance, the effect of turbulence becomes important only when σ^2 >10-4. There is a general tendency for performance to diminish with decreasing array spacing. The reason is that small arrays have small phase differences between the elements, and these small differences are more difficult to detect above the noise.

Another very noticeable feature for both models is a peak in the CRLB (i.e., poor array performance) when $2d/\lambda \approx 10$ (~ $\approx \mathcal{L}$). This peak results from the fact that most of the turbulent energy occurs around the scale $\mathcal{L}$. When the spacing is much larger than $\mathcal{L}$, the phase differences between the sensors are large enough that turbulence has little effect. When the array spacing is much less than $\mathcal{L}$, the phase fluctuations tend to be uniform across the array, and hence do not diminish performance. The von Kármán model suggests a greater sensitivity to turbulence at small spacings than the Gaussian model, because it (more realistically) contains more small-scale turbulent energy (see Fig. 5).

---

[1] The direction of tower-based spectral measurement is effectively the along-wind direction. The time series for the turbulent fluctuations is converted to a spatial series by setting $\Delta x = UAt$, where U is the wind speed.

[2] Array performance is best at broadside incidence. When the wavefronts are perpendicular to the array axis, the CRLB becomes infinite.

Gaussian scalar model

he scalar Gaussian model is defined by the following correlation function:

$$R(r)=\sigma^2\exp\left(-\frac{r^2}{L^2}\right),$$

where σ^2 is the variance, and L is the Gaussian length scale. The corresponding energy spectrum is

$$E(\kappa)=\frac{\sigma^2\kappa^2L^3}{4\sqrt{\pi}}\exp\left(-\frac{\kappa^2L^2}{4}\right),$$

and the two-dimensional correlation function is

$$b(\rho)=\frac{\sigma^2L}{2\sqrt{\pi}}\exp\left(-\frac{\rho^2}{L^2}\right).$$

The Gaussian length scale and integral length scale $\mathcal{L}$ are related by

$$\mathcal{L}=\frac{\sqrt{\pi}}{2}L\cong 0.886L.$$

von Kármán scalar model

The scalar von Karman model is defined by the following energy spectrum:

$$E(\kappa)=\frac{41(17/6)}{3\sqrt{\pi}\Gamma(1/3)}\frac{\sigma^2\kappa^4\ell^5}{\left(1+\kappa^2\ell^2\right)^{17/6}},$$

where σ^2 is the variance, and ℓ is the von Karman length scale. The corresponding correlation function is

$$R(r)=\frac{2\sigma^2}{\Gamma(1/3)}\left(\frac{r}{2\ell}\right)^{1/3}\left[K_{1/3}\left(\frac{r}{\ell}\right)-\left(\frac{r}{3\ell}\right)K_{2/3}\left(\frac{r}{\ell}\right)\right],$$

where K_ν is the modified Bessel function. The two-dimensional correlation function is

$$b(\rho)=\frac{4\sigma^2\ell}{3\sqrt{\pi}\Gamma(1/3)}\left(\frac{\rho}{2\ell}\right)^{5/6}\left[K_{5/6}\left(\frac{\rho}{\ell}\right)-\left(\frac{\rho}{2\ell}\right)K_{1/6}\left(\frac{\rho}{\ell}\right)\right].$$

The von Karman length scale and integral length scale $\mathcal{L}$ are related by

$$\mathcal{L}=\frac{2\sqrt{\pi}\Gamma(5/6)}{311113)}\ell\cong 0.498\ell.$$

Kolmogorov scalar model

Define the structure function for the scalar N as

$$D(r)=\left\langle\left[N(r)-N(0)\right]^2\right\rangle.$$

The structure-function parameter is

$$C_N^2=\lim_{r\to 0}D(r)/r^{2/3}.$$

The approximate energy spectrum (valid for $k\mathcal{L}>>1$) is

$$E(\kappa)=\frac{2^{5/3}}{11\sqrt{\pi}}\frac{\Gamma(17/6)}{\Gamma(2/3)}C_N^2\kappa^{-5/3}\cong 0.207C_N^2\kappa^{-5/3}$$

The approximate two-dimensional structure function (valid for $r/\mathcal{L}<<1$) is

$$d(\rho)=\frac{\Gamma(1/6)}{5\sqrt{\pi}\Gamma(2/3)}C_N^2\rho^{5/3}\cong 0.464C_N^2\rho^{5/3}.$$

Wilson and Thomson model

The Wilson and Thomson semi-empirical model (*J. Acoust. Sot. Am, 96.* 1080) *is the* sum of six Gaussian correlation functions, representing:

1. small-scale temperature fluctuations
2. small-scale velocity fluctuations (along wind)
3. small-scale velocity fluctuations (cross wind)
4. temperature / velocity covariance
5. large-scale velocity fluctuations (along wind)
6. large-wale velocit y fluctuations (cross wind)

The model incorporates some observed features of anisotropy characteristic of atmospheric turbulence.

For most common daytime conditions the small-scale velocity fluctuations dominate. For propagation downwind, the twc-dimensional correlation is then

$$b(\rho)=\frac{6.3\sigma^2L}{2\sqrt{\pi}}\left(1-\frac{\rho^2}{L^2}\right)\exp\left(-\frac{\rho^2}{L^2}\right),$$

where $L=zz$, and $\sigma^2=222u_*^2/c_0^2$. The 6.3 is an anisotropy factor, resulting from vortex stretching due to wind shear.

Figure 4. Basic results for several turbulence models. More complete derivations, including the vector forms of the models, can be found in Wilson (1997a).

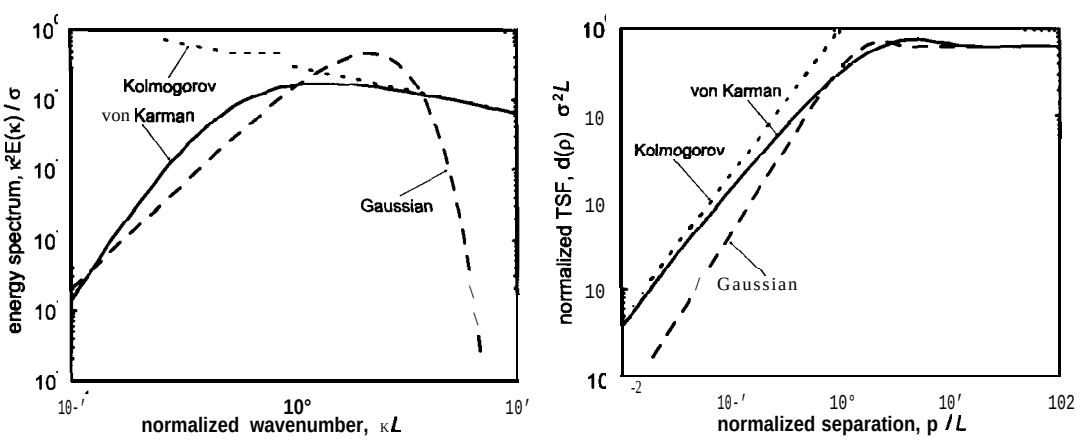

Figure 5. Comparison of the scalar Gaussian, von Kármán, and Kolmogorov models. On the left are the energy spectra, and on the right are the 2D correlation functions (TSF's). The energy subrange corresponds to $\kappa\mathcal{L}<<1$ and $\rho/\mathcal{L}>>1$, and the inertial subrange to $\kappa\mathcal{L}>>1$ and $\rho/\mathcal{L}<<1$.

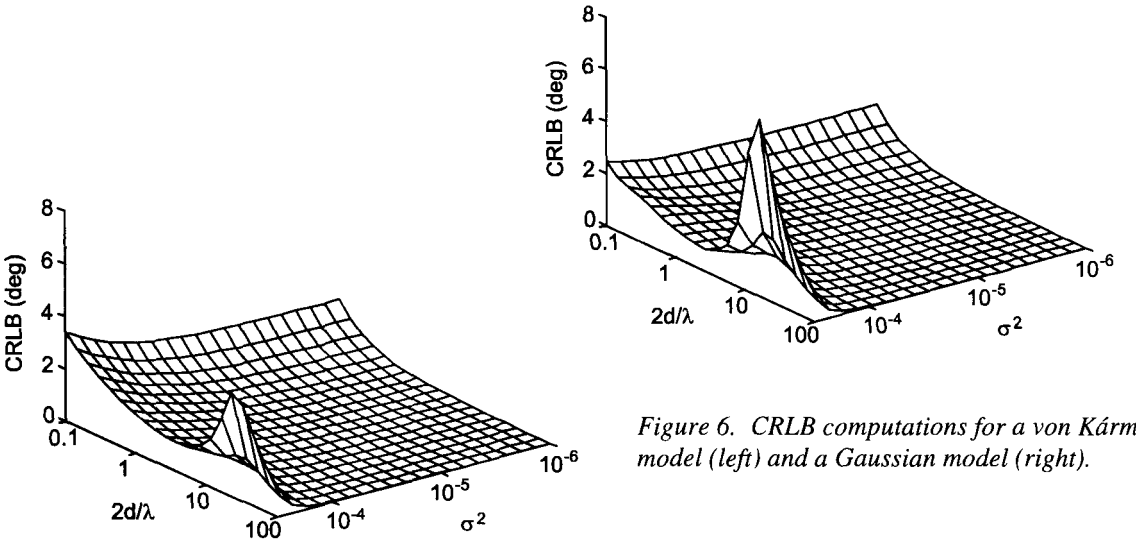

Figure 6. CRLB computations for a von Kármán model (left) and a Gaussian model (right).

The four turbulence models are compared in Fig. 7. The variance was set to $22u_*^2/c_0^2$, where u_* is the friction velocity, and the Gaussian length scale was set to z (Wilson and Thomson, 1993). The length scale needed for the von Kármán model can be determined from the integral length scale, which is known from the Gaussian scale (Fig. 4). The Kolmogorov model parameters can be determined from the inertial subrange asymptote of the von Kármán model.

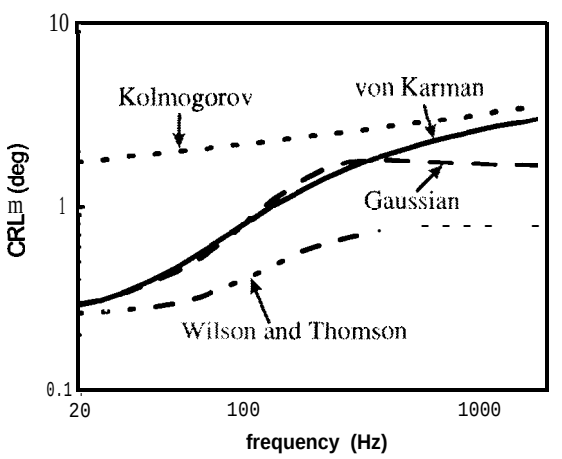

Figure 7. Comparison of the four turbulence models for windy atmospheric conditions.

The meteorological parameters used in the creation of Fig. 7 were typical of a windy, neutral atmosphere: $u_* = 05$ m/s, $T_* = -0.01$ K, and z_i (the inversion height) = 1000 m. The interelement array spacing was one-half wavelength, the propagation distance was 500 m, the array height was 2 m, and SNR was 20 dB.

All of the models except for the Kolmogorov one lead to similar results at very low frequency. The Kolmogorov model performs well only above 1000 Hz or so. The Gaussian and von Kármán models agree well up to several hundred Hz. At this point they diverge, because the Gaussian model does not have a realistic inertial subrange. The reason why the isotropic Gaussian and Wilson and Thomson models diverge above 20 Hz or so is due to the anisotropy factor present in the latter. The Wilson and Thomson model contains a factor of 6.3 representing the stretching of eddies in the direction of the wind. Overall we see that the von Kármán model is the only one that behaves reasonably well for all frequencies, although it does not capture anisotropic effects that are evidently important.

Figure 8 shows MCF and CRLB predictions for the Wilson and Thomson model as a function of the meteorological conditions. The computations use the same parameters as in Fig. 7, although the frequency has been fixed at 200 Hz, and u_* and T_* were varied. It is evident that the turbulence effect depends more strongly on u_* than

on T*, implying wind shear-generated turbulence plays a more important role than thermal structure. Hence it is often justifiable to neglect the effect of temperature fluctuations.

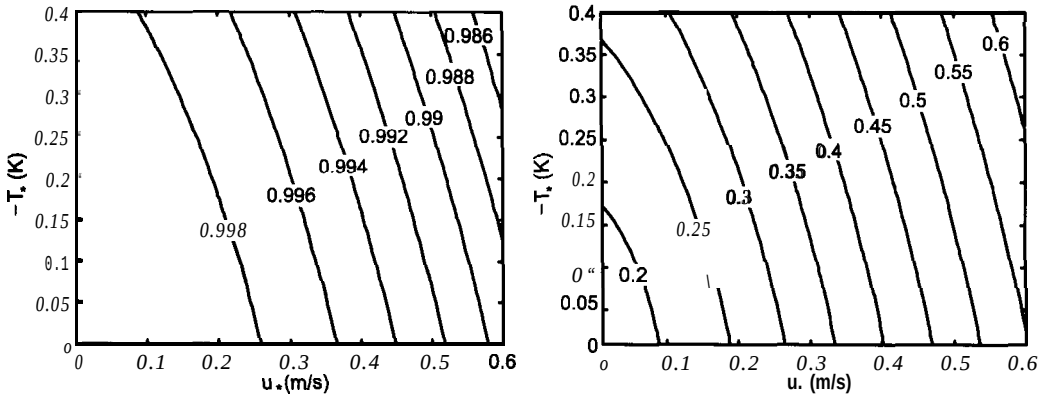

Figure 8. Dependence of the MCF (left) and the CRLB (right) on the turbulence scaling parameters u_* and T_*.

7. Turbulent Intermittence

The analysis in the previous section implicitly assumed that the strength of the turbulence (e.g., the variance or the structure-function parameter), averaged over the length of the propagation path, was constant. Although this is a standard assumption, it is probably not a good one. In actuality the statistical properties of a turbulent flow, even when the flow may be considered homogeneous and stationary, are a local property of the averaging region *unless the* region is large compared to the external scales associated with the flow. In the atmosphere, the relevant external scale is the boundary-layer inversion height, which is on the order of 1 km. Hence, unless an acoustical system operates over scales of many kilometers, the variation in local turbulence properties could be significant.

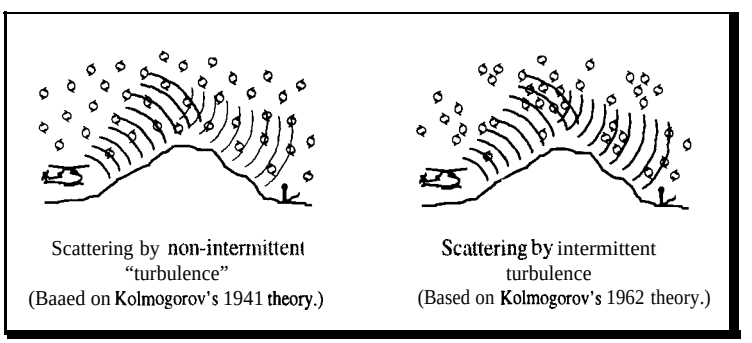

Figure 9. Scattering from both the non-intermittent and intermittent viewpoints. The strength of the turbulence is depicted (non-rigorously) by the concentration of eddies.

This characteristic of turbulence statistics, called *intermittence,* was first described systematically by Kolmogorov (1962). An illustration of the effect is given in Fig. 9. So far very little research has been done on incorporating intermittence effects into theoretical treatments for propagation through turbulence. This is a significant oversight from the standpoint battlefield acoustics, and probably also for many EM scenarios. Among the few authors who have consider intermittence effects on wave propagation are Gurvich and Kukharets (1986) and Tatarskii and Zavorotnyi (1985).

We can account for intermittence in the Kolmogorov model simply by using a structure function parameter $\tilde{C}_v^2$ that is *local* (average) to the propagation path, in place of its ensemble mean $C_v^2 = \langle \tilde{C}_v^2 \rangle$ (Tatarskii and Zavorotnyi, 1985). (Tildes are used here to indicate local parameters.) The resulting local MCF is

$$\tilde{\Gamma}\left(\rho, \tilde{C}_v^2\right) \cong \exp\left\{-0.21\pi k^2 X \tilde{C}_v^2 \rho^{5/3}\right\}$$

The local structure function parameter has an approximately log-normal distribution (Kolmogorov, 1962). That is, $\ln \tilde{C}_V^2$ is approximately normal. It can be shown (Wilson, 1997b) that $\tilde{C}_V^2$ is less than $\exp\left(\ln\langle\tilde{C}_V^2\rangle - 2.15\sigma_V^2\right)$ 5% of the time, and greater than $\exp\left(\ln\langle\tilde{C}_V^2\rangle + 1.15\sigma_V^2\right)$ 95% of the time, where σ_V^2 is the variance of $\ln \tilde{C}_V^2$. These particular values for $\tilde{C}_V^2$ are called the 5% lower and 95% upper confidence bounds, respectively. The log-mean and log-variance parameters can be estimated from the following formulas (Wilson, 1997b):

$$\langle\tilde{C}_V^2\rangle \approx 2\left\langle\frac{u_*^3}{0.4z}\right\rangle^{2/3}, \quad \sigma_V^2 \approx 0.16\ln\left(\frac{0.3z_i}{X}\right),$$

where z is the height. (These parameterizations assume a neutral atmosphere.)

An example calculation of the MCF and its confidence bounds is shown in Fig. 10. The non-intermittent MCF curve corresponds to $\tilde{\Gamma}\left(\rho,\langle\tilde{C}_V^2\rangle\right)$. The lower 5% confidence bound for the MCF is just $\tilde{\Gamma}$ evaluated at the lower570 bound for $\tilde{C}_V^2$ given above, and likewise for the upper 95% bound. The actual mean MCF is $\langle\tilde{\Gamma}\left(\rho,\tilde{C}_V^2\right)\rangle$. The computations are for a frequency of 100 Hz, propagation distance 100 m, and inversion height 1000 m. The index-of-refraction variance was 2 x 10^{-5}. The figure shows that the actual mean MCF is not all that different from the MCF calculated using the non-intermittent theory. However, the non-intermittent theory does neglect substantial variability in the MCF. At $\rho/\mathcal{L}$=0.02, for example, coherence varies between approximately 0.2 and 0.95. When the wind is momentarily weak, and hence the wind-shear generated turbulence is momentarily weak, excellent coherence is obtained; a strong gust nearly wipes out the coherence.

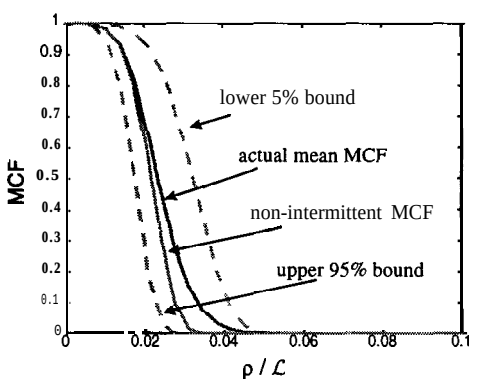

Figure 10. Example calculations of the MCF in intermittent turbulence using the Kolmogorov model.

CRLB calculations, as a function of frequency and propagation distance, are shown in Fig. 11. For these calculations, u_*=0.5 m/s and z=2 m. The SNR was 20 dB and the interelement spacing was 1 m. When the CRLB is plotted in this manner, it is nearly independent of propagation distance near to the source and at low frequency. This is the region where array performance depends mostly on the noise environment. As the frequency and distance are increased, however, the CRLB increases sharply. This is the turbulence effect. The turbulence effect is only minimally significant for momentarily weak winds (the 5% lower bound), but becomes dominant in most cases during a strong gust (the 95% upper bound). At 80 Hz and 1000 m, for example, the CRLB fluctuates between 0.6 and 2 deg. Tracking schemes should be designed to take advantage of this effect, by locking onto the source during the episodes of weak turbulence, and maintaining the track during temporary dropouts due to strong turbulence.

8. Conclusions

When an acoustic array is positioned near to a source, its ability to produce accurate AOA estimates and hence track the source is limited primarily by the noise present. As the distance is increased, however, turbulence takes over as the limiting factor in AOA accuracy. The transition typically occurs at about 100 m for a frequency 100 Hz and SNR 20 dB.

A lack of good, 3D turbulence models hinders accurate predictions of the performance of acoustic arrays. The main modeling difficulty is the anisotropy occurring at large scales. Although imperfect, the von Kármán model

appears to be the best overall choice for now. Gaussian and Kolmogorov models can both be very misleading, since they work well for only certain subranges of the turbulence.

Wind velocity fluctuations caused by near-ground wind shear are almost always the most important source of turbulent degradation in AOA estimates. Significant variation in the intensity of these wind fluctuations occurs as the wind intermittently weakens and gusts. This intermittence can cause the accuracy of the AOA estimates to fluctuate dramatically.

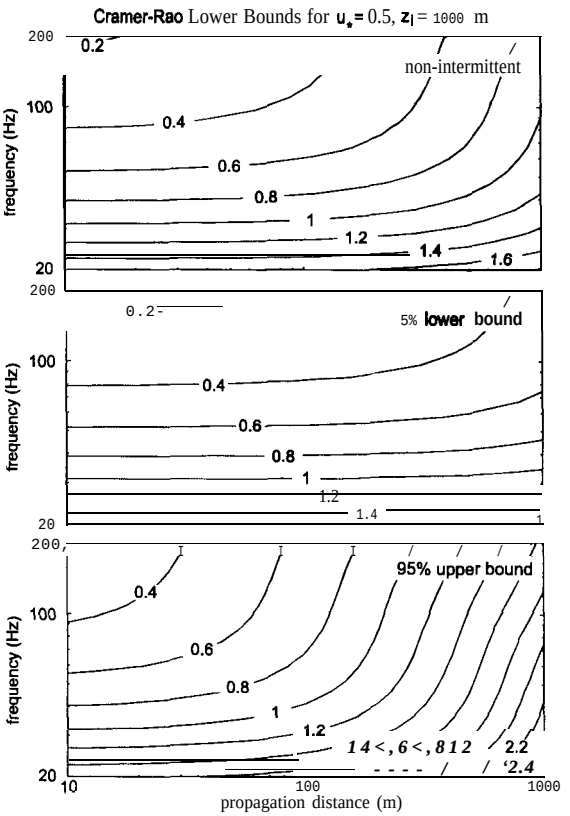

Figure 11. CRLB calculations (in deg) showing the effect of turbulent intermittency. The calculation in the top box is for the non-intermittent case. The middle and bottom boxes are the 5% lower and 95% upper confidence bounds, respectively (i.e., the CRLB fluctuates so that it is between the two bounds 90% of the time).

References

Batchelor, G. K. (1953): *The Theory of Homogeneous Turbulence.* Cambridge University Press, Cambridge, Great Britain.

Gurvich, A. S., and V. P. Kukharets (1986): The influence of intermittence of atmospheric turbulence on the scattering of radio waves. Sov. *J. Comun. Technol. Electron. 30, 52–58.*

Kolmogorov, A. N. (1962): A refinement of previous hypotheses concerning the local structure of turbulence in a viscous incompressible fluid at high Reynolds number. *J. Fluid Mech. 13, 82–85* (1962).

Ostashev, V. E. (1994): Sound propagation and scattering in media with random inhomogeneities of sound speed, density, and medium velocity. *Waves Rand. Med. 4, 403-428.*

Rytov, S. M., Y. A. Kravtzov, V. I. Tatarskii (1989): *Principles of Statistical Radio Physics, Part 4: Wave Propagation through Random Media.* Springer, Berlin.

Song, B. G., and J. A. Ritcey (1996): Angle of arrival estimation of plane waves propagating in random media. *J. Acoust. Sot.* Am. 99, 1370-1379.

Tatarskii, V. I., and V. U. Zavorotnyi (1985): Wave propagation in random media with fluctuating turbulence parameters. *J. Opt. Sot. Am. A 2,2069-2076.*

Wilson, D. K., and D. W. Thomson (1993): Acoustic propagation through anisotropic, surface-layer turbulence. *J. Acoust.* Sot, Am. 96, 1080-1095.

Wilson, D. K. (1997a): Turbulence models for wave propagation and scattering calculations. Technical report, U.S. Army Research Laboratory, 2800 Powder Mill Road, Adelphi, MD 20783. (In preparation.)

Wilson, D. K. (1997b): Performance bounds for acoustic angle-of-arrival arrays operating in atmospheric turbulence. Submitted to *J. Acoust. Sot. Am.*